2018

Scour from bidirectional current flows around offshore monopoles

Mackinnon, T.

*The Plymouth Student Scientist, 2018, **11**, (2), 217-243*

Scour from bidirectional current flows around offshore monopoles

Thomas Mackinnon

Project Advisor: Jon Miles, School of Engineering, University of Plymouth, Drake Circus, Plymouth, PL4 8AA

Abstract
Two tests for a unidirectional and bidirectional current were applied to a 100mm, cylindrical Perspex monopile and the surrounding bathymetries were measured using an industry standard laser profiler traverse system. It was observed the maximum scour depths for a bidirectional current were 47% larger the unidirectional current. The equilibrium scour depth was also predicted by four previously derived equations by other researchers. This found all four significantly over predicted the unidirectional maximum scour depth; however, the bidirectional current was more accurately predicted, with only a 1.5% error against a modern unidirectional prediction. Results identify bidirectional temporal scour development requires further research as the point of equilibrium is not fully agreed upon.

Introduction

This report will compare the maximum scour hole depths and shapes between unidirectional and bidirectional currents for a scaled model windfarm monopile. An industry leading traverse and laser profiling system has been adopted to provide detailed surface profiles at multiple stages in the scour development, highlighting the differences of scour shape and maximum depth between unidirectional and bidirectional currents. The results are then compared against predictions for both unidirectional and bidirectional currents, finding the results varied significantly.

Monopiles are slender, cylindrical, hollow, steel foundations that penetrate deep into the seabed to act as foundations for towers such as offshore wind turbines. They are best suited in shallow to intermediate water depths, up to 30m. Alternatives to monopiles include gravity based and jacket foundations, respectively, these are less expensive and better in deep waters greater than 30m; however, they are both limited by the quality of seabed conditions. Monopiles are a more versatile and preferable design as they avoid the limitations of the bed's strength because they transmit loads directly into the marine bedrock. Causes of failure for monopiles include foundation instability and the exposure of essential equipment, such as power cables, buried in the seabed. A previous cause of mass windfarm failure was an insufficient grouting strength between the foundational monopile and wind turbine tower in 2012 (Vriees, 2010). This failure caused an estimated industry loss of £25.2million due to ceased wind energy production and difficult site locations for repair (Price, 2012). This therefore highlights the requirement for full design understanding to minimise maintenance costs in the difficult offshore site conditions.

Seabed scour is a term used instead of 'erosion' to distinguish the process of sediment transport caused by the presence of a structure in the marine environment (Sumer & Fredsøe, 2002). Monopile scour has been thoroughly researched in regards to bridge pier design for unidirectional, one-way, flowing rivers (Hjulström, 1935; May et al., 2002; Melville, 2008; Melville & Chiew, 1999). However, physical processes unique to coastal conditions, such as waves or tidal currents, are yet to be fully understood. Recent research has been investigating the influence of waves on scour hole generation, such that the variable is now included with significance in leading scour prediction equations (Zanke et al., 2011). It is therefore possible bidirectional, two way, currents will cause an equally variable maximum scour depth and shape, which is an essential design parameter to understand for efficient and safe equipment burial depths, such as windfarm power cables.

Literature Review

Scour Processes

Scour occurs when the velocity of a current exceeds the critical velocity required to initiate sediment movement, often identified for steady currents by the Shields parameter (Hamill, 2011) shown equation 1.

$$\theta = \frac{\tau_\infty}{\rho g d_{50}(s-1)} \quad (1)$$

Where τ_∞ is the undisturbed bed shear stress in a current; d_{50} is the sediment grain size; g is the acceleration due to gravity; s is the specific gravity of sediment grains, and ρ is the water density.

The presence of marine structures, such as monopiles, constrict the water currents through a reduced cross section, this induces an increased current velocity when passing the pile (Raudkivi, 1998). Predictions for the current acceleration can be modelled theoretically, shown White (1991) and Acheson (1990). If the increased velocity exceeds the critical velocity, shown equation 1, then sediment movement occurs and a scour hole begins to form (Hamill, 2011). Scour around a pile is exacerbated by vortex effects that uplift sediment for easier transportation (May et al., 2002). Horseshoe vortices spiral along a horizontal axis at the pile base and sides. They are formed when currents first encounter a monopile as they are forced down towards the pile base; becoming turbulent and spiralling horizontally due to the adverse pressure gradients induced by the structure (Sumer & Fredsøe, 2002) (Hamill, 2011). At the rear of the pile, lee-wake vortices form and spiral along a vertical axis due to shear forces along the pile sides. Lee-wake vortices often extend downstream of the pile, causing longitudinal scour holes (Hamill, 2011; Sumer & Fredsøe, 2002; May et al., 2002). Sediment accretion can occur downstream of the pile due to sediment depositing after the flow returns to a laminar, subcritical velocity. Accretion can also occur at the immediate rear the pile due to the pile partially sheltering it from the current and vortices (Hamill, 2011).

Seabed State

The velocity of the current can already exceed the critical velocity required for sediment transport without the need for marine structure influence, these conditions are divided into live-bed, clear-water and wash-load states. A live-bed seabed state is experiencing a flow velocity greater than the required shear force (equation 1) to initiate sediment movement or entrainment in the flow; resulting in continuous sediment transport all along the seabed and creating sediment input into areas of scour (Raudkivi, 1998). A clear-water state is experiencing a flow velocity less than the required sediment shear force, so sediment transport and scour infilling is not occurring (Raudkivi, 1998). Regardless of the previous two states, wash-load can occur, this is the transportation of suspended fine sediment or debris in the water and it can increase the scouring effect by exerting a higher shear force than normal flow (Raudkivi, 1998).

Melville (2008) summarises findings from Chiew (1984), Ettema (1976, 1980) and Baker (1986) observing the differences between clear and live bed conditions for cylinder bridge piers with variable sediment uniformities under unidirectional currents. For uniform sediments, maximum scour depth occurs in clear water conditions when $\boldsymbol{v}/\boldsymbol{v_c} \approx$ 1.0, where $\boldsymbol{v}$ is the mean current velocity, and $\boldsymbol{v_c}$ is the critical mean current velocity for sediment entrainment. As $\boldsymbol{v}$ increases, equilibrium scour depth decreases before rising to a secondary peak in live bed conditions when $\boldsymbol{v}/\boldsymbol{v_c} \approx$ 4.0, however the maximum live bed scour depth is less than the clear water conditions. As the uniformity of the sediment decreases, the clear water peaks at

significantly smaller maximum scour depths, whereas the live bed peak remains constant. Therefore, as the uniformity of a sediment decreases, the maximum scour depths are only achieved in live bed conditions.

Sheppard, et al. (2006) finds similar shaped results as Melville (2008) for scour depth at all seabed states and across all sediment uniformities, however the data does not repeat the trough that is between the clear water and live bed peaks

Flow Shallowness

The depth of the water body for marine structures has been shown to influence maximum scour depths in shallow water conditions (May et al., 2002; Melville, 2008). In deep water conditions, the dominant scouring vortex at the front and sides of the pile are horseshoe vortices; however, during shallow water conditions the generation of horseshoe vortices can be significantly inhibited by surface rollers that behave similarly to horseshoe vortices, but rotate in the opposite direction at the water surface (Melville, 2008). Therefore, in shallow water conditions the magnitude of scour is reduced due to fewer and smaller horseshoe vortices. May et al. (2002) identifies the depth at which surface rollers significantly influence the generation of horseshoe vortices when $h/D < 3$. Shallower water depths shown to reduce the maximum equilibrium scour in laboratory testing includes Breusers et al. (1997); Yu (2016); Chiew (1984); Escarameia & May (1999) and Raudkivi (1986). Escarameia & May (1999) observed an 83% decrease in equilibrium scour depths for a 50% reduction in relative flow depths under bidirectional currents.

Unidirectional Currents

Unidirectional current scour has undergone significant historic research, partially due to its relevance to bridge pier design on riverbeds. Matutano et al. (2013) summarises seven prominent formulae for predicting maximum scour depths for steady unidirectional currents and/or waves. These formulas were proposed by Breusers et al. (1997); Zanke (1982); Melville (1988); Sumer (1992); Richardson (1995); Sumer & Fredsøe (2002); and Zanke (2011).

Research began initially with just steady current flows, and based on empirical data and previous testing Breusers et al. (1997) produced an initial formula for predicting maximum equilibrium scour depth for a cylindrical pile, shown equation 2.

$$\frac{H}{D} = 1.5D \times \tanh\left(\frac{h}{D}\right) \quad (2)$$

Where H is the maximum scour depth; D is the diameter of the monopile; h is the water depth to the seabed.

Zanke (1982) published equation 3 based on a semi-analytical approach, including the dependency of sediment motion on the mean velocity of a current; based on Hjulström's curve (1935) on critical velocity required for sediment motion, shown equation 4. Zanke (2011) highlights from observations by Link (2006) and testing by Sheppard, et al. (2006) that the curve over predicts data if live-bed current speeds are stopped before scour depth is measured.

$$\frac{H}{D} \approx 2.5\left(1 - 0.5\frac{u_c}{u}\right) \quad (3)$$

$$u_c = 1.4\left(2\sqrt{\rho' g d_{50}} + 10.5\frac{v}{d_{50}}\right) \quad (4)$$

Where u_c is the maximum critical velocity for sediment motion, ρ' is the relative density ($\rho' = (\rho_s - \rho)/\rho$) , and v is the kinematic viscosity of the fluid.

Melville (1988) proposed $H/D = 2.4$ as the maximum possible scour depth for cylindrical piles; however, this depth could be reduced by factors associated to sea state conditions, flow shallowness and sediment size. Sumer (1992) refined this relationship to $H/D = 1.3$ for general cases. Whitehouse (2011) collected scour depths from 10 European windfarms, finding the maximum scour depths occurring at Scroby Sands, ranging between $H/D = 0.95$ to 1.38, suggesting Sumer (1992) is an appropriate predication.

Later research by Sumer & Fredsøe (2002) and Zanke (2011) included the influence of waves on maximum scour depths. They incorporated the KC number, which is a dimensionless number to describe the relative significance between inertia and drag forces induced by the wave conditions. Both papers agreeing KC > 6 result in negligible scour changes; originally discussed by Sumer et al. (1992, 1993) and Kobayashi & Oda (1994). Zanke (2011) applied the factor to equation 3, maintaining the influence of u_c/u; whereas Sumer (1992) applied it to $H/D = 1.3$, with no inclusion of u_c/u.

Sheppard et al. (2014) evaluated 23 recent and commonly used equilibrium scour equations for cohesionless sediments against both lab and field results. The accuracy of each equation was numerically assessed with focus on the least overall error and least under prediction. Of the 23 predictions, only 17 demonstrated enough accuracy to be worth observation, with a general trend of increasing accuracy over the years. Finding Breusers et al. (1997) was 11th most accurate, underestimating the maximum scour depths at only 4% of field points. Contrastingly, Matutano, et al. (2013) performed a similar analysis for Breusers et al. (1997) and an equation based on Sumer et al. (1992); finding 80% of predictions underestimated the maximum scour depths at prototype European windfarms (Whitehouse, 2011).

Bidirectional Currents

Bidirectional currents have undergone significantly less research than unidirectional currents, however past data has shown there is cause for further investigation. Bidirectional currents are used to simulate prototype tidal currents, which typically cycle over 12.3 hours from an inwards to outwards current, denoted as ebb and flow currents, respectively. For simplicity, most tidal currents are simplified to a two-way bidirectional, with a constant current, whereas prototype astronomical tide conditions follow a sinusoidal current speed change with a gradual 180° change in direction. Escarameia & May (1999) states scour depths about a cylinder monopile for bidirectional currents was greater than unidirectional currents. These results were

observed to occur up to 4 - 5 half-tidal cycles of current, approximately 2.0 – 2.5 model hours. Escarameia & May (1999) state that at this 2.5-hour point, the bidirectional scour hole stabilised in maximum scour depth, however their provided data does not appear to agree if it equalised gradually like the unidirectional current. The data plots provided show an equal, if not steeper, rate of scour than unidirectional flow prior to the 2.5-hour point, therefore indicating the tidal scour is unlikely to have stabilised that rapidly, when the unidirectional current continued to increase in scour depth for an additional 30 hours. After 4 hours of current, the unidirectional scour depth reaches the same scour depth as the bidirectional at 2.5 hours, showing scour rate was significantly less for the unidirectional currents during the first 5 half cycles of a bidirectional test.

The bidirectional currents were scaled for a 12.3-hour tidal cycle, however Escarameia & May (1999) observed the largest equilibrium scour depths occurred during the shorter tidal cycles. Furthermore, some testing included the growth of tidal flow velocity as a sinusoidal curve to better simulate prototype astronomical tide conditions, these tests were found to produce approximately 90% of the maximum scour depths under the same conditions. From testing, two equilibrium scour depth equations were produced for both unidirectional and bidirectional currents for various piles shapes; these equations for circular piles are shown equations 5, 6 and 7.

Unidirectional Equilibrium Scour Prediction (Escarameia & May, 1999):

$$H_{uni} = 2.53\left(\frac{h}{D}\right)^{0.6}\left(1 - 3.66\left(1 - \frac{u}{U_c}\right)^{1.76}\right) \quad (5)$$

Bidirectional Equilibrium Scour Prediction (Escarameia & May, 1999):

$$H_{bi} = \left(1.80 - 0.24\frac{D_T}{T_{50}}\right)H_{DT} \quad for\ 0.55 \leq \frac{D_T}{T_{50}} \leq 2.5 \quad (6)$$

$$H_{bi} = 1.2H_{DT} \quad for\ \frac{D_T}{T_{50}} > 2.5 \quad (7)$$

Where T_{50} is the characteristic time, D_T is the duration of the equivalent tide at constant critical velocity, and H_{DT} is the estimated scour depth after the first half cycle.

Yu (2016) assessed the difference in scour profiles for composite bucket foundations under unidirectional and bidirectional currents, observing a 16% reduction in equilibrium scour depth for bidirectional currents. Furthermore, the bidirectional current reached equilibrium scour depth at approximately 28 hours, whereas unidirectional stabilised at approximately 36 hours, supporting the point Escarameia & May (1999)'s bidirectional scour holes may not have stabilised so rapidly at 2.5-hours.

Scaling Errors

Scaling a model from prototype conditions can produce a multitude of scaling errors. Generally, monopile scour experiments utilise a Froude scaling over Reynolds scaling (Yu, 2016; Escarameia & May, 1999; Sumer et al., 1993), because turbulence is considered a significant cause of scaling error. During laboratory testing, an accurately scaled sand size for most models displays non-physical sediment movement for prototype conditions, such as high cohesion or extreme mobility/suspension. Therefore, it is standard practice to adopt a fine sand, such as G_f 0/1 (Escarameia & May, 1999; Zanke et al., 2011; Yu, 2016). The implications of an improperly scaled grainsize has been theorised to produce larger equivalent scale depths than experienced in prototype conditions (Sheppard et al., 2004; Lee & Sturm, 2008).

Sheppard et al. (2004) investigated the effect of D/d_{50} on maximum scour depths in clear water conditions; showing through multiple pile sizes; sediment d_{50}'s; current speeds and water depths that there was a functional dependence of scour depth to the ratio of pile width and sediment grain size. Similar to Lee & Sturm (2008), Sheppard et al. (2004) found maximum scour depths of H/D = 2.5 were achieved at $D/d_{50} \approx 25$. Lee & Sturm (2008) additionally tested changes to of D/d_{50} on live-bed sea states, observing the maximum scour stabilises from $D/d_{50} > 100$ to H/D = 1.2; with the most significant relationship occurring at Fr < 0.4. Lee & Sturm (2008) theorise this dependency is attributed to the large pours of the comparatively large sediment grains dissipating the horseshoe vortices, therefore inhibiting a key process of sediment uplift/scour.

Froude's Equation for Critical Flow:

$$Fr = \frac{V}{\sqrt{gh}} \tag{8}$$

Temporal Scour Development

Scour depth develops gradually overtime, eventually reaching a quasi-equilibrium state close to the maximum scour depth. Melville & Chiew (1999) observed the temporal development of scour in unidirectional currents for clear water seabed states; finding 80% of scour occurred between 5 – 40% of the total time required to reach an equilibrium scour depth. Melville & Chiew (1999) additionally describe clear water temporal scour development as asymptotic; therefore identifying the point of equilibrium scour depth as when the scour depth increases less than 5% of the pile depth in 24 hours. During live-bed states, Sheppard et al. (2006) found scour equilibrium would not behave asymptotically, reaching the maximum scour depth within a matter of hours, continuing to oscillate around an equilibrium depth.

For bidirectional flows, Yu (2016) and Escarameia & May (1999) observed scour development followed an oscillating process around the pile. Yu (2016) recorded the maximum scour would occur consistently at one point, which oscillated up and down while following a generally linear growth in scour depth before reaching an equilibrium at 28 hours. Escarameia & May (1999) observed a linear generation of maximum scour depth before stating it stabilised rapidly by the fifth half-tidal cycle.

Methodology

The experiment was performed in a 20m x 0.6m wave flume in a sand box with dimensions 2m x 0.32m hanging flush with the flume bed.

Initial Set-up

While the flume was empty, the sandbox was uncovered and filled with uniformly graded G_f 0/1 fine sand, shown Figure 2. Once the sediment was flush with the flume base, water filled the flume to a depth of 150mm, measured with a ruler. An impeller was placed in the water at the end of the flume, approximately 6m from the sand box. The flume's current pump was activated and steadily increased in power until the 'ebb' current measured an average speed of 0.2 m/s on the impeller readout; the pump percentage power was recorded. This was then repeated for a reverse direction, 'flow', current. An industry standard traverse was then set up by aid of the lab technicians, with the laser profiler fixed to the end, set up shown Figure 3 and Figure 4. The model plastic monopile with male to female separator was securely placed in the centre of the sand box, shown Figure 5, with its base in contact with the sandbox base. The grid resolution of the traverse was then tested for non-collision while the monopile was separated, shown Figure 6. The sand bed was then smoothed by eye to approximately level, shown Figure 7 and Figure 8, and the laser was calibrated.

To calibrate the laser voltage to the distance from the seabed, the traverse system was submersed to approximately 70mm from the seabed. The traverse then withdrew away from the sand bed at 10mm intervals, recording 10 voltage readings with the laser profiler at each point, results shown Figure 1. Figure 1 shows a linear correlation between the distance from the seabed to voltage measured. The equation of the linear trend line, shown equation 9, shows the calibrated distance per measured voltage is 27.276mm. The R^2 value, shown equation 10, is very close to 1.0; therefore, identifying equation 9 describes the data fit with a strong correlation and is an appropriate calibration of the equipment.

$$y = 27.276x + 567.5 \quad (9)$$

$$R^2 = 0.9999 \quad (10)$$

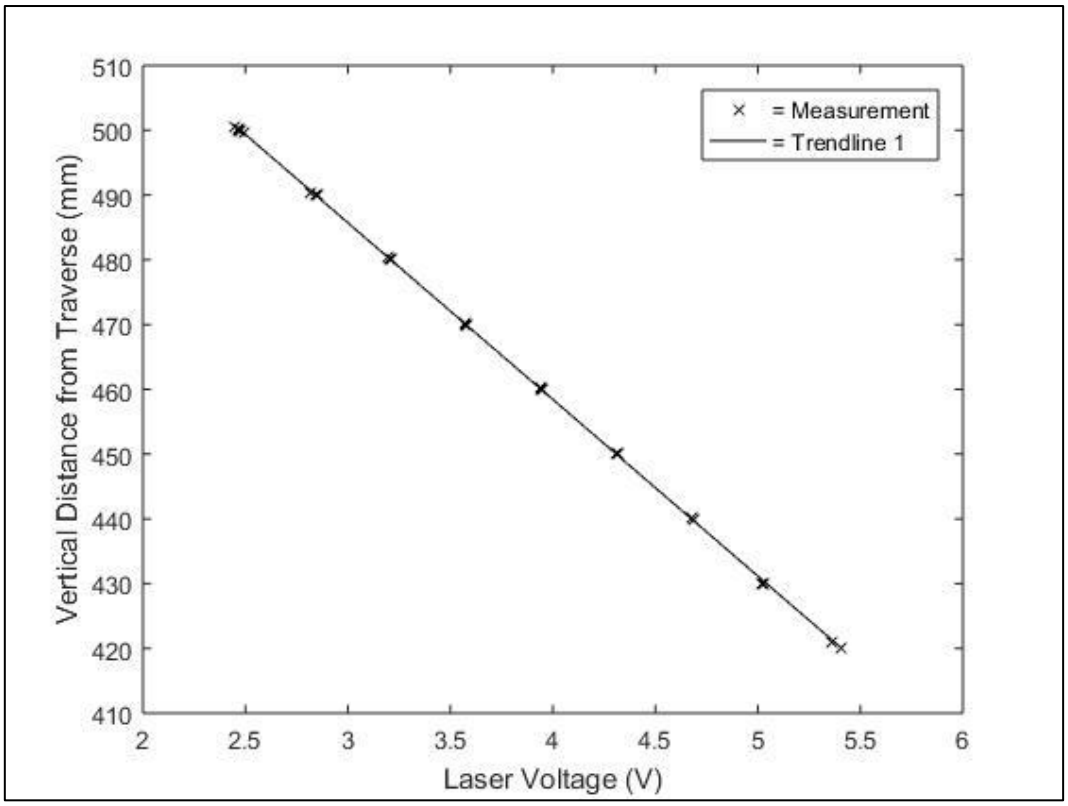

Figure 1: Laser voltage calibration

Figure 2: Sandbox being filled with sand

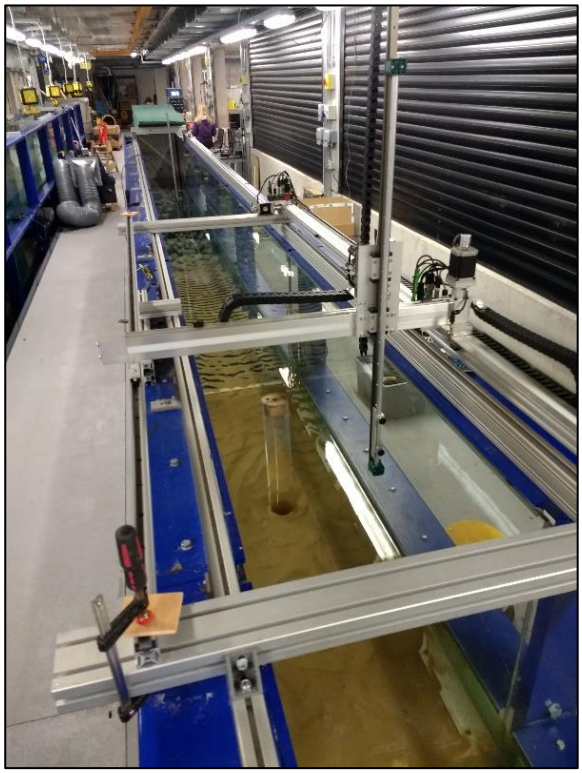

Figure 3: Final traverse set-up

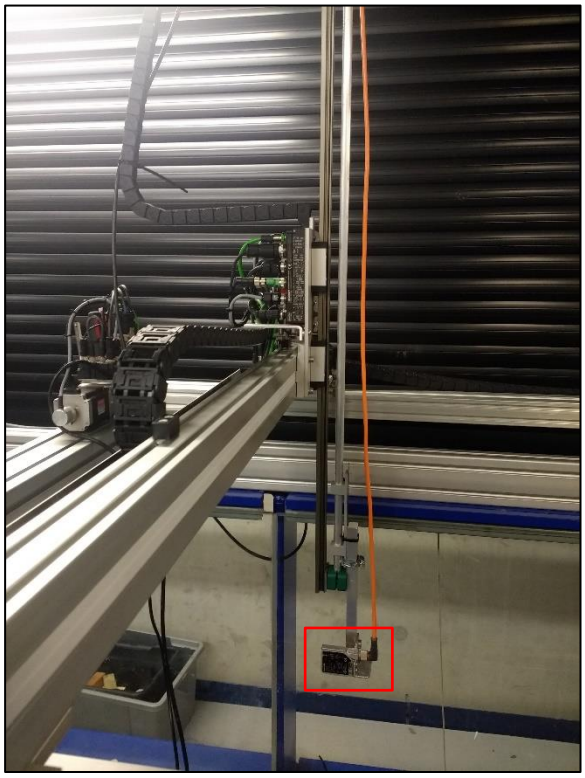

Figure 4: Traverse arm with laser profiler end piece (laser highlighted red)

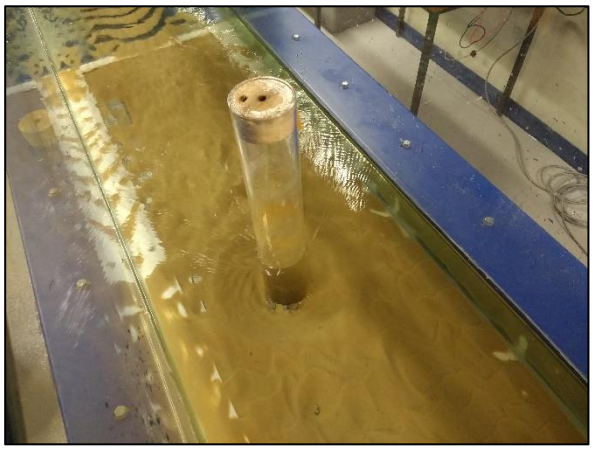

Figure 5: Example test conditions

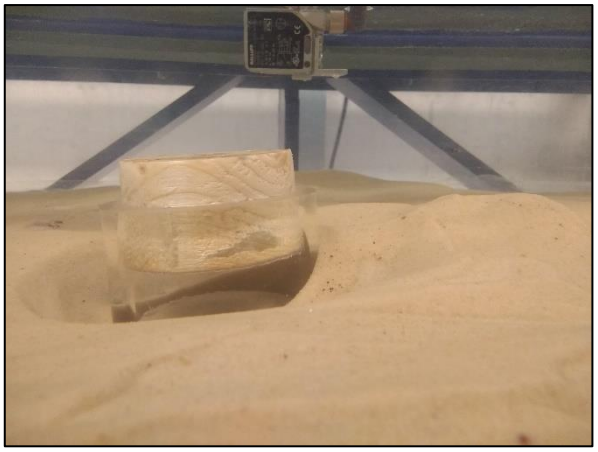

Figure 6: Laser profile clearance over detached monopile

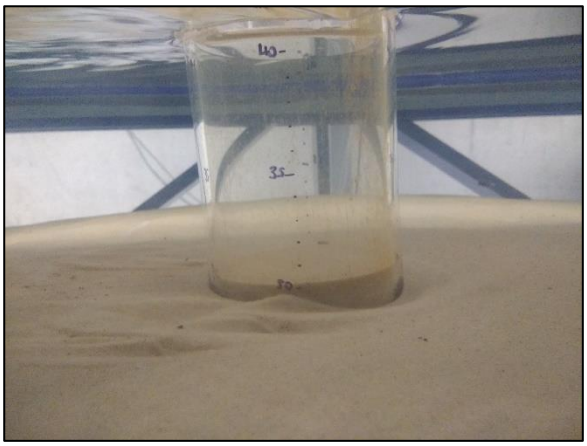

Figure 7: Close up of monopile to sand bed boundary before testing

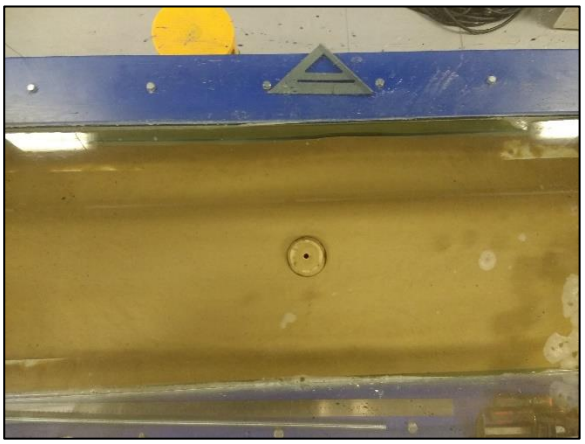

Figure 8: Lay out of conditions before testing

Traverse Scan Set-up

The traverse system required co-ordinates for points to measure scour depth, these co-ordinate grids are shown Figure 9 and Figure 10. For Test 1 scans 0 – 60 minutes, the 20x20mm grid was used; for Test 1 scans 90 – 150 minutes and Test 2 scans 0 – 240 minutes, the 10 x 20mm grid was used. The vertical Z co-ordinates remained constant through test 1 and 2 at 460mm from the traverse's upper boundary; this maintained consistency; that the laser profiler was always fully submerged, and at no risk of colliding with the monopile. At each coordinate point, the traverse paused for 2 seconds, allowing time for the traverse to become stationary and the laser profiler to measure an average from five voltage readings. When not in use, the traverse system withdrew from the water to co-ordinates x=0, y=0, z=0 so to minimise its risk of damage or test interference.

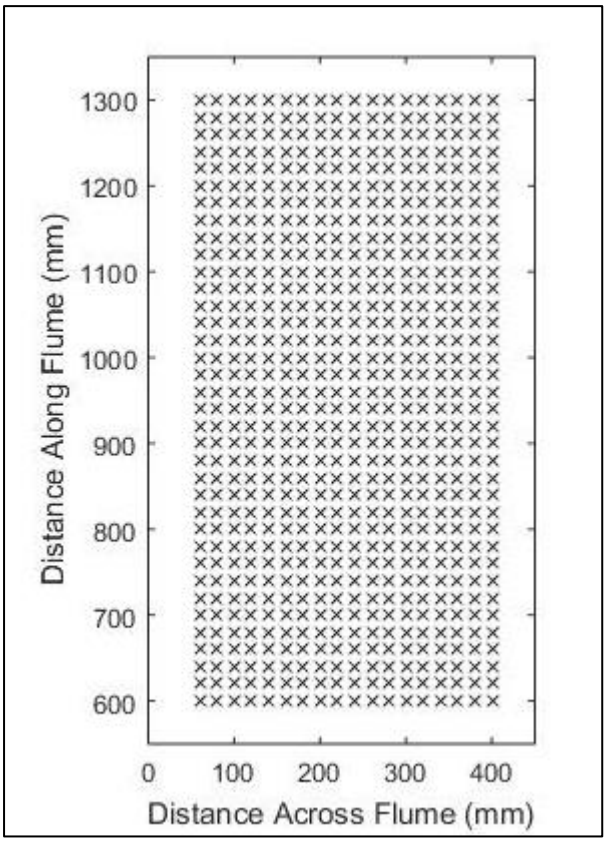

Figure 9: 20 x 20mm grid resolution

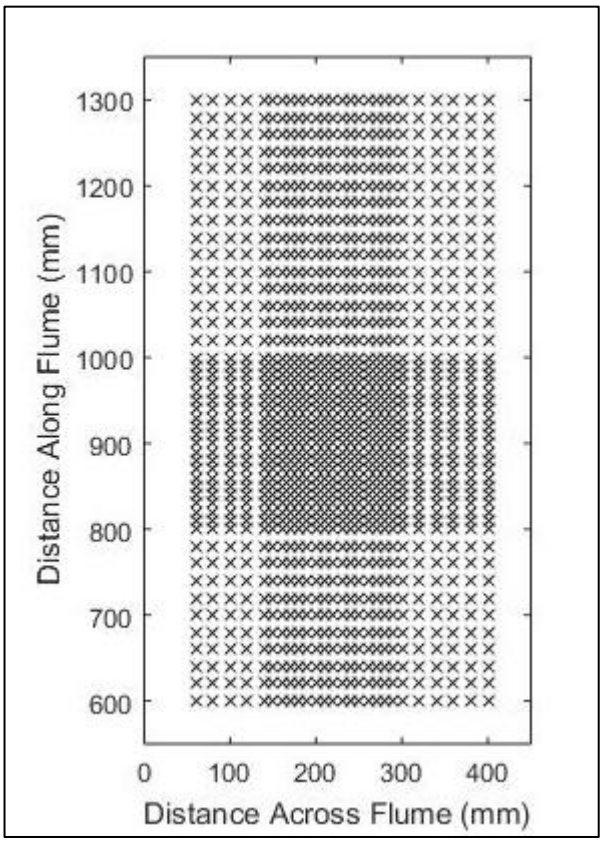

Figure 10: 10 x 20mm higher resolution grid over scour pit

Test 1 – Unidirectional Flow
The seabed was smoothed to approximately level and an initial traverse scan at 0 minutes was performed before a current was applied. A 0.2m/s 'ebb' current was then applied for 30-minute intervals, with traverse scans performed between each 30-minute current. This was repeated 5 times, until a total current time of 150 minutes had elapsed. During current flows, the average current speed was confirmed at 0.2m/s by the impeller readout. Before each traverse scan, the top piece of the pile was carefully removed, with the sediment formations undisturbed.

Test 2 – Bidirectional Flow
The seabed was smoothed to approximately level and an initial traverse scan at 0 minutes was performed before a current was applied. A 0.2m/s 'ebb' current was then applied for a 60-minute interval, then a 0.2m/s 'flow' current was applied for a 60-minute interval in the opposite direction. Traverse scans were performed between each 60-minute current. The 'ebb' and 'flow' currents were then repeated an additional time, as described above, ending after a total current time of 240 minutes had elapsed. Before each traverse scan, the top piece of the pile was carefully removed, with the sediment formations undisturbed.

Test 3 – Temporal Scour Development
The seabed was smoothed to approximately level. A measurement scale along the pile length, shown Figure 7, was drawn by ruler from the pile base at 0°, 90°, 180° and 270° around the pile perimeter. A 0.2m/s 'ebb' current was then applied for 60-minutes, and the distance from the monopile base at the front, rear and side of the pile was recorded at 2-minute intervals.

Results

Test 1 - Surface Plots for a Unidirectional Flow

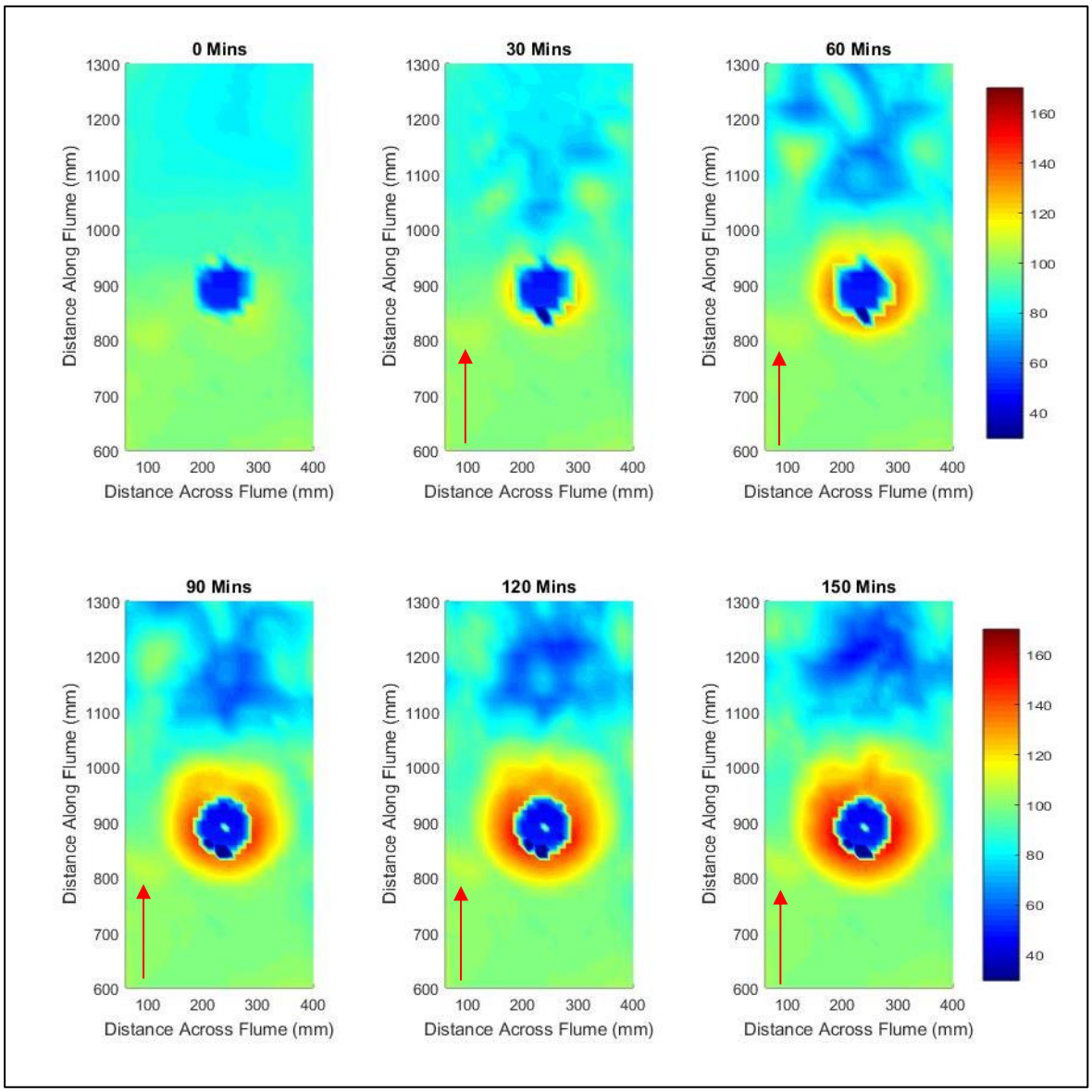

Figure 11: (Colour) Unidirectional flow surface scans, red arrow indicating the direction of current flow that interval.

Figure 11 shows a gradually increasing scour hole size, depth and rear sediment accretion with each 30-minute increment of current. Upstream of the monopile, the bathymetry of the sand bed remains largely undisturbed and constant, with no deposition or scour changes outside the range of the scour hole. The final scour hole diameter at 150 minutes is approximately 240mm, with the immediate front and sides of the pile possessing similar maximum scour depths. The immediate rear of the pile experiences a slight reduction in scour compared to the sides, with a visible ‘tail’ of scour protruding from the rear.

Test 2 - Surface Plots for a Bidirectional Flow

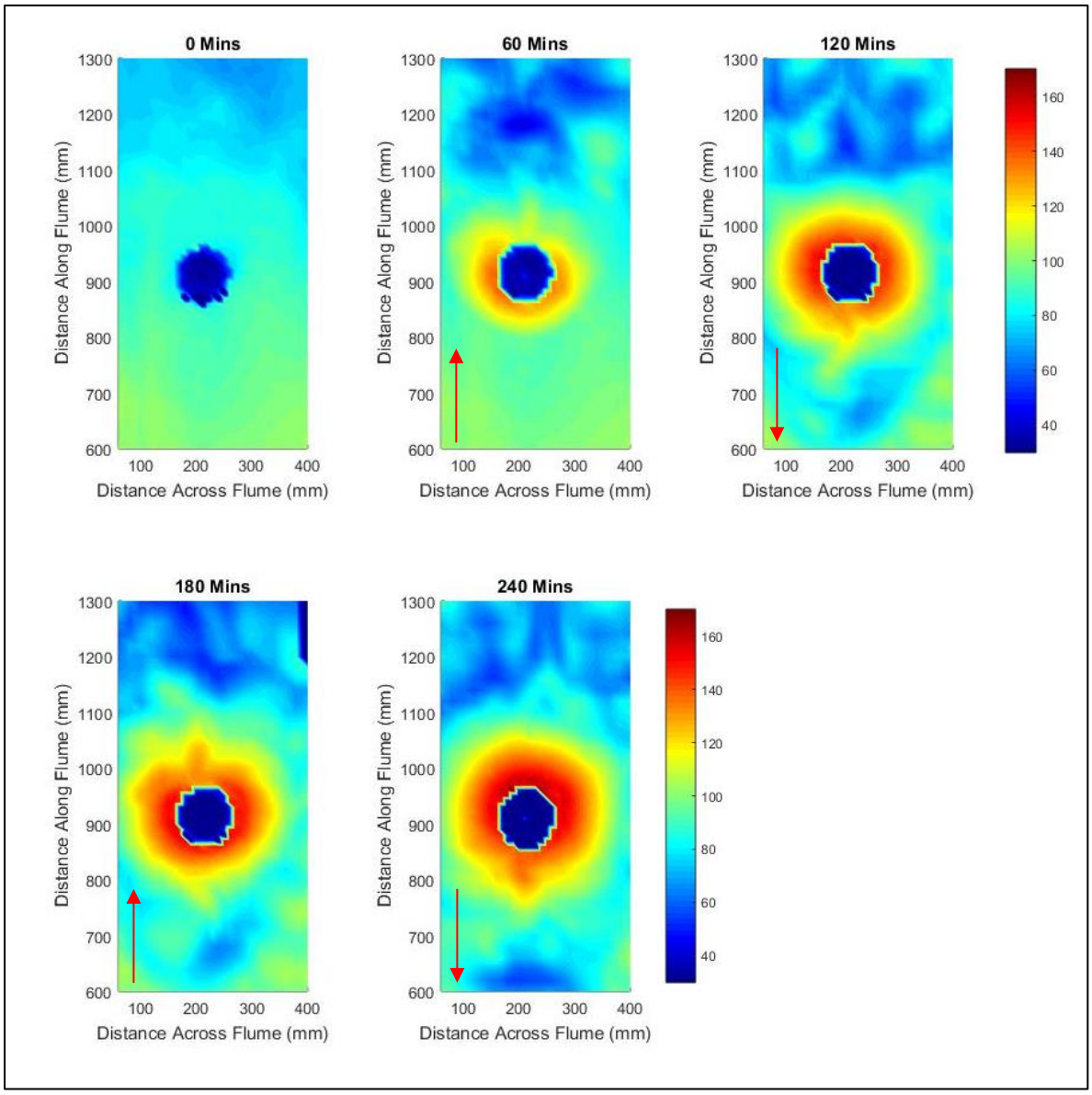

Figure 12: (Colour) Bidirectional flow surface scans, red arrow indicating the direction of current flow for that interval.

Figure 12 shows a gradually increasing scour hole size, depth and rear sediment build up with each 60-minute increment. The initial 60-minute ebb flow reveals a similar scour shape to test 1; with a width of 180 mm, however a scour 'tail' is already forming. After the reverse flow current at time 120-minutes, the scour 'tail' has flipped position to the new pile rear, with sediment accretion now occurring behind it on the previously flat bed. After each current direction change, the previous rear sediment deposit breaks down in size and shape. The final scour hole diameter at 240 minutes is approximately 280mm, with the maximum scour depth at the pile front.

Test 1 - Unidirectional Centreline Section Seabed Profile

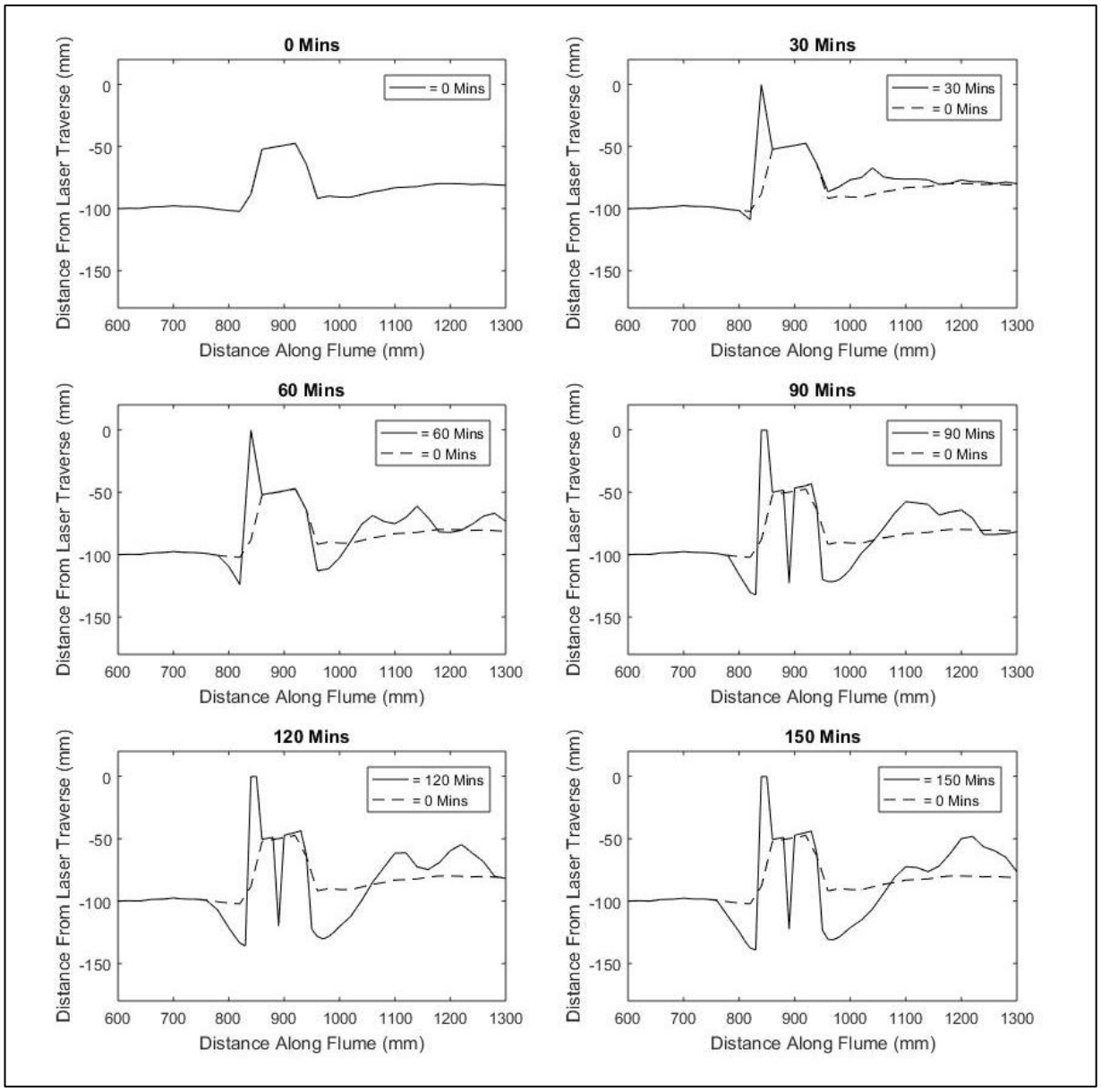

Figure 13: Unidirectional section of the seabed profile through the centreline of the monopile for each current time step, red arrow indicating the direction of current flow for that interval.

Figure 13 shows a gradually increasing scour hole size, depth and rear sediment build up with each time increment. Maximum scour depth and gradient steepness occurs at the front of the pile for all time steps, with the rear always slightly less. Although maximum scour depth appears to begin stabilising between scans 120 – 150 minutes, the rear sediment deposition, scour hole size and gradient continue to change. The maximum scour depth of 36mm occurs at 150 minutes, with a maximum rear sediment deposition of 27mm.

Test 2 - Bidirectional Centreline Section Seabed Profile

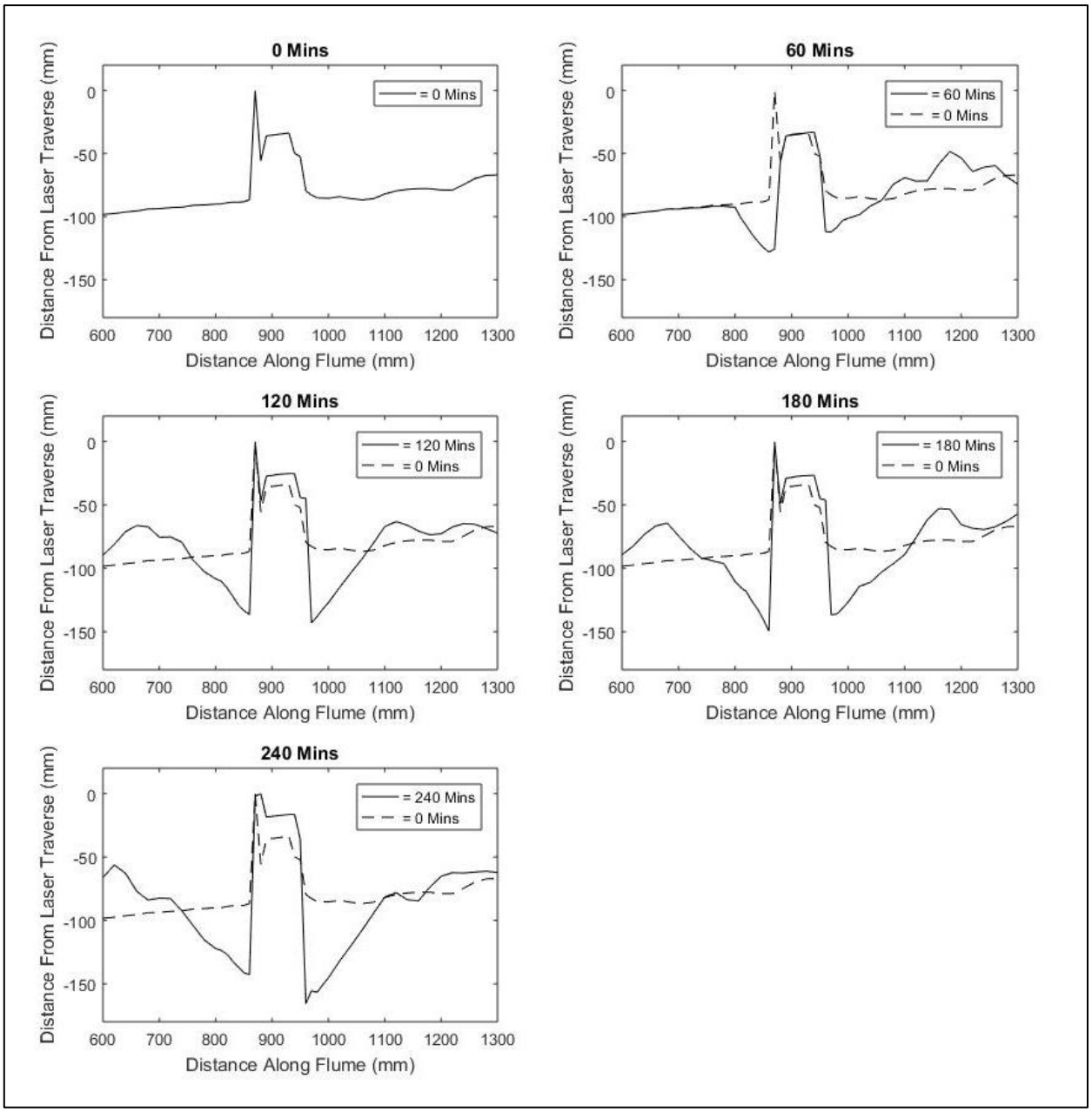

Figure 14: Bidirectional section of the seabed profile through the centreline of the monopile for each current time step, red arrow indicating the direction of current flow for that interval.

Figure 14 shows a gradually increasing scour hole size, depth and rear sediment build up with each time increment. Maximum scour depth occurs at the front of the pile, towards the current, therefore switching sides for each time step/current direction. Sediment deposition at the rear changes in size and shape after each current change, often smoothing to fewer deposit peaks. The maximum scour depth of 73mm occurs at 240 minutes, with a maximum rear deposition of 46mm.

Test 3 - Temporal Scour Development

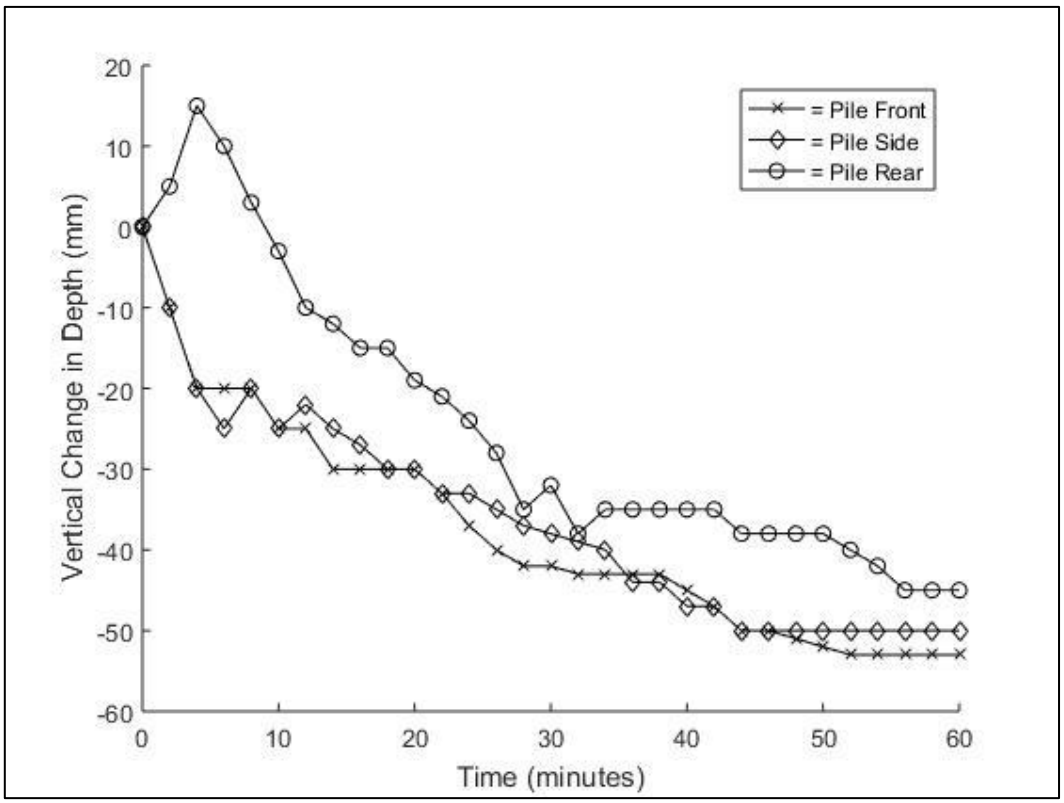

Figure 15: Temporal scour hole depth development at the pile perimeter for a unidirectional flow

Figure **15** shows a gradual increase in maximum scour depth for the front, side and rear of a pile. The front and sides of the pile immediately begin to scour from 0-minutes, whereas the pile rear accretes sediment for the initial 4 minutes of current. The rate of scour for all points initially occurs rapidly, 0-6 minutes for the front and sides, 4-12 minutes for the rear, before the rate of scour slows. Maximum scour depth of 53mm occurs at the front of the pile from 52 minutes, whereas the minimum scour depth of 45mm occurs at the pile rear at 56 minutes. After the initial rear accretion, scour occurs at a similar rate for all points.

Maximum Scour Depths

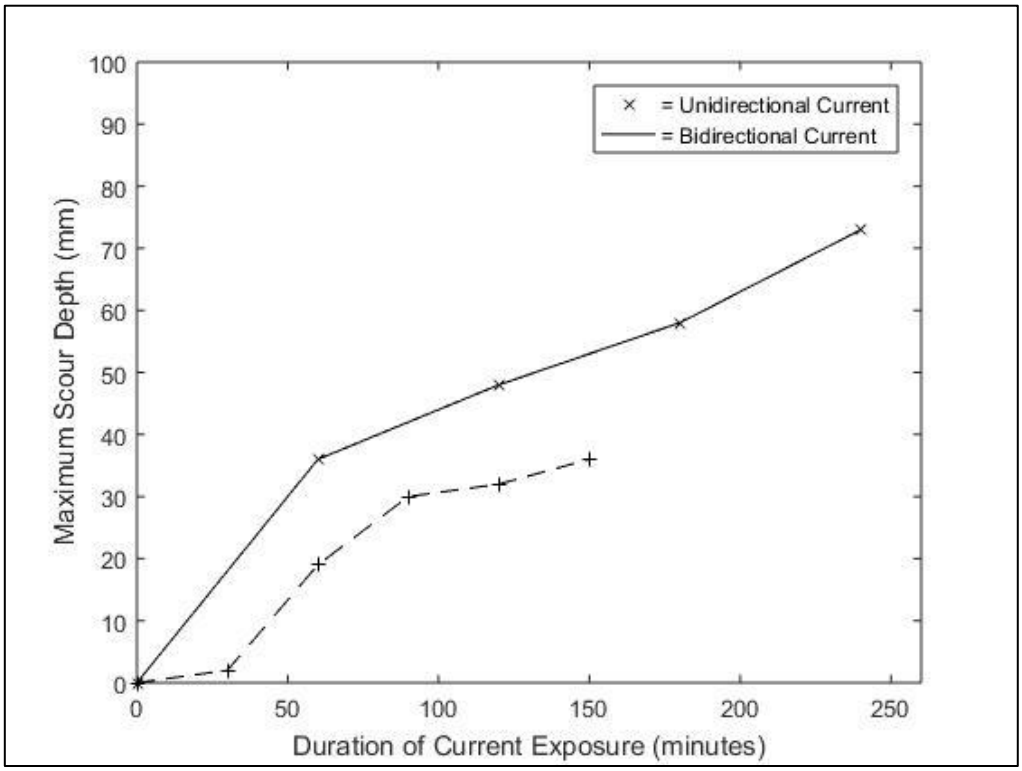

Figure 16: Maximum temporal scour depth from test 1 and 2

Figure 16 shows scour depth gradually increasing with time for both the unidirectional and bidirectional currents. At all measurements, the bi-directional current is at least 40% larger than the unidirectional current. The rate of scour begins to decrease after 90 minutes for test 1's unidirectional flow, whereas test 2's bidirectional scour remains at both a higher and constant gradient for the rest of the test.

Comparison of Predictions

Table 1 shows a significant range of scour depths. Test 2's bidirectional current closely matching Zanke's steady flow prediction, equation 3, with a 1.5% difference. Test 1's unidirectional current is significantly less than Zanke's prediction with a 51% difference. Equations $H/D = 2.4$ (Breusers et al., 1997) and 1.3 (Sumer et al., 1992) are both significantly larger than test 1 and 2, up to 560% difference from test 1 to $H/D = 2.4$ (Breusers et al., 1997). Escarameia & May (1999) is additionally larger than the bidirectional flow, by approximately 35% for test 2.

Table 1. Table of measured maximum scour depths and predicted maximum scour depths calculated from

Data Source	Maximum Scour Depth (mm)
(Zanke, et al., 2011)	74
H/D = 2.4 (Breusers et al., 1997)	240
H/D = 1.3 (Sumer et al., 1992)	130
(Escarameia & May, 1999)	99
Test 1 Unidirectional	36
Test 2 Bidirectional	73

Visual Observations

Throughout the experiment, linguoid sand ripples were generated along the seabed behind the rear of the monopile. The ripples were tallest, steepest and most frequent at the monopile rear, gradually reducing in size and frequency to a negligible bathymetry change 500mm downstream of the pile. During test 2, the reverse flow currents would partially reverse the curvature directions of the sand ripples.
During currents, the pile was observed to create wake and horizontal vortices at the sides, rear and front of the pile; visible due to the disruption along the sand surface and movement of the current's wash load.

Calculations

Prototype to Model Scaling

To ensure industry relevant results the model was based on current monopile prototype installations from local European locations (Whitehouse, 2011).

Table 2. Prototype parameters from eight windfarms around the UK in the North and Irish Sea (Whitehouse, 2011).

Site	Seabed Sediment Type	Monopile Diameter (m)	Peak Current Speed (m/s)	Lowest Water Depth (m)
Scroby Sands (UK)	Medium sand, some gravel/shell	4.2	1.65	3.0
Arklow Bank (Ireland)	Loose to medium dense sand and sandy gravel	5.0	2.00	2.0
N7 pile (Netherlands)	Fine, medium dense sand	6.0	0.75	5.2
Scarweather Sands (UK)	Medium to fine shelly sand	2.2	1.10	6.0
Otzume Balje inlet (Germany)	Medium sand	1.5	1.40	11.7
Barrow OWF (UK)	Fine to muddy sand	4.8	0.80	12.0
Kentish Flats OWF (UK)	Fine sand	5.0	0.90	3.0
North Hoyle OWF (UK)	Gravelly medium sand	4.0	1.17	6.0
All Averaged	**Medium sand**	**4.1**	**1.22**	**6.1**

The averaged parameters were rounded to whole numbers for ease of experimentation and material sourcing, shown Table 3. It was not essential to use the exact prototype average because the site parameters have a high range. A Froude scaling was adopted because turbulence was the largest expected cause for scaling error; as well as the bidirectional current was time dependent; and Froude scaling was adopted by other researchers (Escarameia & May, 1999; Sheppard et al., 2006; Sumer et al., 1992; Yu, 2016; Zanke et al., 2011).

Table 3. Scaling calculations and method from prototype to model

Parameter	Scaling (S=1:40)	Prototype	Model
Monopile Diameter (m)	S	4	0.100
Peak Current Speed (m/s)	S^0.5	1.25	0.200
Lowest Water Depth (m)	S	6	0.150
Sediment grain size	N/A	Medium sand	Fine sand
Single current duration	S^0.5	6 hours	60 minutes

Zanke Equilibrium Scour Depth

$$u_c = 1.4\left(2\sqrt{\rho' g d} + 10.5\frac{v}{d}\right) = 0.281\ m/s \quad (11)$$

$$H_{equ} = 2.5D\left(1 - 0.5\frac{u_c}{u}\right) = 0.74\ mm \quad (12)$$

Escarameia & May Scour Depth

$$H_{DT} = S_{50}\left(\frac{D_T}{T_{50}}\right) = 82mm \quad (13)$$

$$H_{eq} = 1.2H_{DT} = 99mm \quad (14)$$

Froude Number

$$Fr = \frac{V}{\sqrt{gD}} = 0.165 \quad (15)$$

0.165 < 1, therefore subcritical flow

Discussion

Unidirectional and Bidirectional Result Comparison

Figure 11 shows the formation of the scour hole and surrounding bathymetry for a unidirectional current conformed with previous laboratory and prototype research, highlighting a rear deposition and steady, circular, scour hole growth (Hamill, 2011; Whitehouse, 2011). Figure 12 shows a similar formation for the bidirectional current to the unidirectional, with a very similar shape from 0 – 60 minutes as test 1, however, with a larger scour hole width of 180mm for bidirectional compared to 150mm for unidirectional. During test 1, the unidirectional currents caused little to no changes in bathymetry upstream of the pile; however during test 2, when the upstream bathymetry of the pile was non-smooth from a previous current, the bathymetry would now change. Test 2's bidirectional scour shape appeared to reverse in direction to conform to whichever direction the current had just been flowing. It is possible this change in upstream bathymetry influenced the turbulence

at the pile; however, this theory would require further research into pile turbulence conditions to validate.

Figure 13 shows the centreline cross section for the unidirectional current. Figure 15 shows the difference in maximum scour depths for the front, side and rear of the pile, with the maximum scour and deposition occurring at the front and rear respectively; therefore supporting the centreline cross section for Figure 13 and Figure 14 was an appropriate location to measure maximum bathymetry changes for the circular pile. Reviewed alongside Figure 16; Figure 13 and Figure 14 show from times 0 – 150 minutes the bidirectional current had larger maximum scour depths than the unidirectional current. The maximum scour depth at 150 minutes for the unidirectional flow was 36mm, whereas the maximum scour depth for the bidirectional flow was interpolated to 53mm, which is a significant 47% larger than the unidirectional maximum scour. This duration was less than 4-5 half tidal cycles and therefore conforms to Escarameia & May (1999)'s data, that the bidirectional current possessed a higher rate of scour to a unidirectional current during the initial 0 – 5 tidal cycles of a bidirectional current. Melville & Chiew (1999) describe clear water temporal scour development for unidirectional flow as an asymptotic process, and Figure 15 shows that both the unidirectional and bidirectional curves are roughly following a similar asymptotic shape, with the unidirectional current already beginning to reduce in scour rate by 150 minutes. As the unidirectional asymptotic curve is already beginning to level off, it suggests the most significant growth in scour depth had already occurred for test 1, possibly up to 80%, despite the short duration (Melville & Chiew, 1999). Yu (2016)'s testing showed bidirectional scour growth occurred almost linearly until equalising with little warning at a time approximately 75% of the unidirectional current; which was approximately 9 half tidal cycles. Escarameia & May (1999) additionally observed a largely linearly scour generation for bidirectional flow, also stating it equalised rapidly, however this equilibrium occurred at a significantly smaller 4 – 5 half tidal cycles. This lack of consensus for temporal scour development under bidirectional currents indicates it is difficult to predict when test 2's bidirectional scour depth would have equalised, due to an insufficient testing duration and variable results from external research. It is possible the bidirectional temporal scour development is occurring similarly to live-bed scour generation for unidirectional flows, which approached equilibrium scour depth in a very short time with little asymptotic behaviour (Sheppard et al., 2006).

Result to Calculated Prediction Comparison

Table 1. Table of measured maximum scour depths and predicted maximum scour depths calculated from Table 2 shows the predicted equilibrium and experimental maximum scour depths for unidirectional and bidirectional currents. For the unidirectional currents, the predicted equations are all significantly larger than the recorded 36mm. The most accurate prediction was by the Zanke et al. (2011) with 74mm, however this is still 100% larger than the observed 36mm. H/D = 2.4 (Breusers et al., 1997) and H/D = 1.3 (Sumer et al., 1992) are significantly larger than the 36mm, producing values so high that even with full scour development it appears unrealistic the experiment would reproduce these depths. It is worth noting H/D = 2.4 (Breusers et al., 1997) was devised as the maximum depth a scour hole can reach, and coupled with Sheppard et al. (2014)'s evaluation finding Breusers, et al. (1997) overestimated the maximum scour depths of 96% of field points, the H/D =

2.4 as a maximum appears correct. Despite Matutano et al. (2013) finding Breusers, et al. (1997) under predicting eight out of ten European windfarm scour depths.

For bidirectional flow, Zanke et al. (2011) was again the most accurate prediction, with a very small 1.5% difference to the 73mm bidirectional maximum depth. Although these are very similar results, as stated in section 6.1, it is very difficult to estimate when the bidirectional scour depth will reach equilibrium due to the linear scour growth rate. Therefore, depending on whether the scour depth conforms at a time similar to Escarameia & May (1999)'s or Yu (2016)'s observations, Zanke et al. (2011)'s prediction may not end up describing the data so closely. Escarameia & May (1999) predicted a final equilibrium depth of 99mm, which is 35% larger than the observed depth. Escarameia & May (1999) expected the scour depth reaching an equilibrium at approximately 4 – 5 cycles; therefore as the bidirectional test was stopped at the fourth tidal cycle, it is unlikely the 99mm scour depth would be reached in the remain half cycle. If however, the bidirectional scour continued to develop similar to Yu (2016)'s observations, its possible Escarameia & May (1999)'s prediction would be quite accurate.

Review of Conditions

The test conditions were based on averaged parameters for prototype European windfarms and standard practice for scour depth laboratory testing. Previous research by Sheppard et al. (2004), Melville (2008) and May et al. (2002) indicates the maximum scour depths for the model monopiles size may not fully represent the prototype maximum scour due to depth, sediment and velocity conditions; this could explain the significant over predictions of Table 2. Sheppard et al. (2004) observed currents with Fr values < 0.4 exhibited a strong relationship of D/d_{50} to maximum scour depth, finding maximum scour depth occurred when $D/d_{50} = 1.0$. This experiment's current possessed a Fr = 0.165, therefore indicating the maximum scour depth could be up to 50% less than was possible due to the large $D/d_{50} = 200$. Despite this, the scaling and sediment size used is representative of other leading research in this field (Zanke et al., 2011; Escarameia & May, 1999; Melville & Chiew, 1999; Yu, 2016), therefore, this condition is considered acceptable and unlikely to have influenced the predictive equations.

Melville (2008) observed similar changes to maximum scour depths depending on the uniformity of the sediment and ratio of current velocity over critical velocity for sediment uplift. This experiment possessed a uniform sediment, therefore maximum scour depth could be observed in clear water conditions at $v/v_c = 1.0$. This experiment had a $v/v_c = 0.71$, which suggests maximum scour depth for this model diameter was not reached. The laboratory parameters were based on prototype conditions with peak currents speeds and variable sediment sizes, therefore this possible scour reduction appears in scale with prototype conditions, and for this baseline test between unidirectional and bidirectional currents induced scour this ratio of v/v_c appears appropriate.

Lastly, May et al. (2002) identified the point at which surface rollers inhibit the growth of horseshoe vortices is $h/D < 3$. This experiment has a $h/D = 1.5$, which suggests scour depth may not have reached its maximum because the horseshoe vortices, which contribute significantly to the scouting process (Hamill, 2011), could not fully form (May et al., 2002). Although this factor cannot fully be confirmed to have

significantly effected the results, both the unidirectional and bidirectional scour was analysed under the same conditions, and therefore the results are consistent.

Limits to Work

During test 1, the scan resolution was initially 20 x 20mm, shown Figure **9**, and refined to 10mm x 20mm grid immediately over the scour pit, shown Figure **10**, beginning after scan 90 minutes, shown Figure 11. This change was essential after realising the 20 x 20mm resolution was insufficiently measuring points of maximum scour immediately around the pile perimeter, as can be seen from the deformed shape shown Figure 13 at time 0 minutes. Due to time constraints, test 1 was not repeated in higher resolution for 0 to 60 minutes. This change prevented the data from being standardised by the original bathymetry. Although it would have been ideal to compare standardised results, the initial bathymetries for test 1 and 2 were very similar, and therefore suitable for comparison.

Future Recommendations

Bidirectional currents were shown to develop varying maximum depths between this report's experimental research and external bidirectional research (Yu, 2016; Escarameia & May, 1999). For future experimentation, it would be beneficial to test several of the conditions investigated for unidirectional currents in bidirectional conditions. These conditions include; the maximum scour depths for different sediment sizes and uniformities; different current velocities between live and clear bed states; full temporal development of bidirectional currents and the influence of waves. Processes unique to bidirectional currents that may influence maximum scour is investigating the difference of sinusoidal velocity growth; and/or a 360° changing current direction to replicate astronomical tidal movement.

Lastly, the traverse functioned extremely well for measuring the bathymetry of the seabed at a 10mm x 20mm resolution. In future experimentation it may be beneficial to increase the grid resolutions up to a maximum of 5mm x 5mm, however, it is possible this resolution would exceed the requirements of the experiment, with the drawback of it producing a significantly longer scan duration, which would reduce the time available for additional experiments.

Conclusions

In conclusion, two tests were performed applying both a bidirectional and unidirectional current to a circular model monopile under the same water depth, sediment size, and current velocities. It was observed that the bidirectional currents produced a 47% deeper maximum scour hole than a unidirectional current for the same time duration of four tidal cycles, 150 minutes. This result differ to previous research comparing the scour of bidirectional and unidirectional currents for circular piles (Escarameia & May, 1999) and bucket foundations (Yu, 2016). Escarameia & May (1999) observed maximum scour growth rate was largest for bidirectional currents; however, the bidirectional currents would reach an equilibrium scour depth significantly earlier than the unidirectional currents, approximately 4 – 5 half cycles, therefore resulting in a smaller equilibrium maximum scour depth. Yu (2016) additionally observed the bidirectional current had a smaller equilibrium maximum scour depth, however it developed linearly and reached an equilibrium at approximate 9 half cycles.

Four predictions were made for the equilibrium scour depths for both unidirectional and bidirectional currents (Breusers et al., 1997; Zanke et al., 2011; Escarameia & May, 1999; Sumer et al., 1992). The most accurate prediction for the unidirectional current was Zanke et al. (2011), however this was 100% larger than the observed 36mm. This prediction was for an equilibrium scour depth, yet although it is clear the unidirectional current had not stabilised, its likely most the scour had developed. This is indicated by the reduced gradient of the curve shown Figure 16, and Melville & Chiew (1999)'s observations that 80% of the scour in clear bed currents would occur in the first 5 – 40% of the time taken for equilibrium scour depth to be reached.

For the bidirectional current, the most accurate prediction was also Zanke et al. (2011) with only a 1.5% difference in scour depth. However, judging by the gradient of the bidirectional curve shown Figure 16, Escarameia & May (1999)'s prediction is most likely to be the most accurate prediction providing the bidirectional scour growth continues after 5 half cycles, unlike Escarameia & May (1999) observed. The experiment was undertaken with parameters based on prototype conditions (Whitehouse, 2011), with standard laboratory practices inducing an acceptable degree of error, such as adopting fine sand. For future research, it is recommended to adopt a laser traverse system due to its efficiency and ease of experimentation. The choice of grid resolution is a trade-off between scanning duration and measurement accuracy; this report found a higher grid resolution immediately over the pile was the most efficient use of time and detail. Lastly, the temporal development of bidirectional scour holes and the changes to current turbulence from upstream bathymetry changes need to be investigated.

Acknowledgements

I would like to thank Jon Miles and the Plymouth University Marine Laboratory staff for their guidance and giving me the opportunity for me to undertake this research project.

References

Acheson, C., 1990. *Elementary Fluid Dynamics,* Oxford: Oxford University Press.

Baker, R., 1986. *Local scour at bridge piers in non-uniform sediment, Report No. 402, 91pp,* Auckland: The University of Auckland.

Breusers, H., Nicollet, G. & Shen, H., 1997. *Local scour around cylindrical piers,* s.l.: J Hydraulic Res IAHR.

Chiew, Y., 1984. *Local scour at bridge piers, Report No. 355, 200pp,* Auckland: The University of Auckland.

Escarameia, M. & May, R., 1999. *Scour around structures in tidal flows,* Wallingford: HR Wallingford.

Ettema, R., 1976. *Influence of bed material gradation on local scour, Report No. 124, 226pp,* Auckland: The University of Auckland.

Ettema, R., 1980. *Scour at bridge piers. Report No. 216, 527pp,* Auckland: The University of Auckland.

Hamill, L., 2011. *Understanding Hydraulics.* 3rd ed. Basingstoke: Palgrave Macmillan.

Hjulström, G., 1935. *Studies of the Morphological Activity of Rivers as Illustrated by the River Fyris,* Uppsala, Sweden: Bulletin Geological Institute Univ.

Kobayashi, T. & Oda, K., 1994. *Experimental study on developing process of local scour around a vertical cylinder,* Reston: ASCE.

Lee, S. O. & Sturm, T., 2008. *Scaling issues for laboratory modeling of bridge pier scour.* Tokyo, s.n.

Link, O., 2006. *An investigation on scouring around a single cylindrical pier in sand (in german).* Mitteilungen des Institutes für Wasserbau und Wasserwirtschaft der Technischen Universität Darmstadt, Heft 136, 117. : s.n.

Matutano, C., Negro, V., Lopez-Gutierrez, J.-S. & Esteban, M. D., 2013. *Scour prediction and scour protections in offshore windfarms,* Amsterdam: Elsevier.

May, R., Ackers, J. C. & Kirby, A. M., 2002. *Manual on scour at bridges and other hydraulic structures.* London: Construction Industry Research & Information Association (CIRCA).

Melville, B., 2008. *The physics of local scour at bridge piers,* Tokyo: 4th Iinternational Conference on Scour and Erosion.

Melville, B. & Chiew, Y.-M., 1999. *Time scale for local scour at bridge piers,* s.l.: Journal of Hydraulic Engineering.

Melville, B. & Sutherland, A., 1988. *design method for local scour at bridge piers,* s.l.: Journal of Hydraulic Engineering.

Price, T., 2012. *Grouting still a major issue for offshore wind.* [Online]
Available at: https://www.renewableenergymagazine.com/wind/grouting-still-a-major-issue-for-offshore
[Accessed 4th December 2017].

Raudkivi, A. J., 1986. *Functional trends of scour at bridge piers,* Reston, Virginia: Journal of Hydraulic Engineering, ASCE.

Raudkivi, A. J., 1998. *Loose Boundary Hydraulics.* Rotterdam: Balkema.

Richardson, E. & Davis, S., 1995. *Evaluating scour at bridges,* Washington DC: USA: Federal Highway Administration.

Sheppard, D., 2004. Overlooked local sediment scour mechanism. *Transportation Research Record,* pp. 107-111.

Sheppard, D., M.ASCE & Miller Jr, W., 2006. Live-bed local pier scour experiments. *Journal of Hydraulic Engineering,* pp. 635 - 642.

Sheppard, D., Melville, B., Demir, H. & M.ASCE, 2014. *Evalutation of existing equations for local scour at bridge piers,* Reston: American Society of Civil Engineers.

Sumer, B., Christiansen, N. & Fredsoe, J., 1992. *Scour around verticle pile in waves,* s.l.: Journal of Waterway, Port, Coastal and Ocean Engineering.

Sumer, B., Christiansen, N. & Fredsoe, J., 1993. *Influence of cross section on wave scouraround piles,* Reston: Journal of Waterways, Ports, Coast and Ocean Engineering, ASCE.

Sumer, B. M. & Fredsøe, J., 2002. *The mechanics of scour in the marine environment.* Singapore: World Scientific.

Vriees, E., 2010. *Slipping Turbines Trigger Investigation into Design.* [Online] Available at: https://www.windpowermonthly.com/article/1006708/slipping-turbines-trigger-investigation-design
[Accessed 20 April 2018].

White, F., 1991. *Viscous Fluid Flow,* New York: McGraw-Hill.

Whitehouse, R., 2009. *Scour at marine structures.* London: Thomas Telford Ltd.

Whitehouse, R. e. a., 2011. *The nature of scour development and scour protection at offshore windfarm foundations.* s.l., HR Wallingford.

Yu, T., 2016. Experimental investigation of current-induced local scour around composite bucket foundation in silty sand. *Ocean Engineering, Vol 117,* pp. 311-320.

Zanke, U., 1982. *Scours at piles in steady flow and under the influence of waves, technical communication 54,* Germany: University of Hannover.

Zanke, U., Hsu, T., Roland A & Diab, R., 2011. *Equilibrium scour depths around piles in noncohesive sediments under currents and waves,* s.l.: Coastal Engineering 58:986-91.